Fei, H., Wiedenbeck, M., Yamazaki, D., Katsura, T. (2014): No effect of water on oxygen self-diffusion rate in forsterite.- *Journal of Geophysical Research*, *119*, 10, p. 7598-7606.

DOI: http://doi.org/10.1002/2014JB011141

AGU PUBLICATIONS

JGR

Journal of Geophysical Research: Solid Earth

RESEARCH ARTICLE
10.1002/2014JB011141

Key Points:
- Water has no effect on oxygen self-diffusion rate in forsterite
- Water effect on olivine rheology is much smaller than previously considered

Supporting Information:
- Readme
- Tables S1–S6

Correspondence to:
H. Fei,
feifei@misasa.okayama-u.ac.jp

Citation:
Fei, H., M. Wiedenbeck, D. Yamazaki, and T. Katsura (2014), No effect of water on oxygen self-diffusion rate in forsterite, *J. Geophys. Res. Solid Earth*, *119*, 7598–7606, doi:10.1002/2014JB011141.

Received 22 MAR 2014
Accepted 2 OCT 2014
Accepted article online 4 OCT 2014
Published online 28 OCT 2014

No effect of water on oxygen self-diffusion rate in forsterite

Hongzhan Fei[1,2], Michael Wiedenbeck[3], Daisuke Yamazaki[2], and Tomoo Katsura[1]

[1]Bayerisches Geoinstitut, University of Bayreuth, Bayreuth, Germany, [2]Now at Institute for Study of the Earth's Interior, Okayama University, Misasa, Japan, [3]Helmholtz Centre Potsdam, Potsdam, Germany

Abstract We systematically measured oxygen self-diffusion coefficients (D_O) in forsterite along *b* crystallographic axis at a pressure of 8 GPa and temperatures of 1600–1800 K, over a wide range of water content (C_{H2O}) from <1 up to ~800 weight ppm. The experimental results suggest that $D_O \propto (C_{H2O})^{0.05\pm0.06} \approx (C_{H2O})^0$. Thus, water has no significant effect on oxygen self-diffusion rate in forsterite. Since the C_{H2O} dependence of silicon self-diffusion rate is also very small, the effect of water on olivine rheology is not significant by assuming the diffusion controlled creep mechanism.

1. Introduction

Water is thought to play an essential role in dynamical processes in the Earth's interior. A number of studies have reported a significant influence for water on the physical properties of mantle minerals, e.g., electrical conductivity [*Karato*, 1990; *Yoshino et al.*, 2009], elastic moduli [*Jacobsen et al.*, 2008], creep rates [*Karato et al.*, 1986; *Karato and Jung*, 2003; *Mei and Kohlstedt,* 2000a, 2000b], atomic diffusivity [*Costa and Chakraborty*, 2008; *Hier-Majumder et al.*, 2005; *Shimojuku et al.*, 2010; *Wang et al.*, 2004], and deformation fabric [*Jung and Karato*, 2001]. In the case of rheological properties, it was believed that even several tens of weight ppm of water could enhance creep rates in olivine by orders of magnitude [*Karato et al.*, 1986; *Mei and Kohlstedt,* 2000a, 2000b]. However, because of the technical difficulty in deformation experiments, the effect of water on olivine rheological properties may have been misunderstood [*Fei et al.*, 2013]. It is necessary to examine the results from deformation experiments independently.

High-temperature creep in minerals is believed to be controlled by self-diffusion of the slowest species [*Frost and Ashby*, 1982; *Weertman*, 1999], which is silicon in the case of olivine [*Costa and Chakraborty*, 2008; *Houlier et al.*, 1990]. Thus, the creep rate can be estimated from the silicon self-diffusion coefficients (D_{Si}). In contrast to deformation studies, *Fei et al.* [2013] demonstrated only a very small effect of water on olivine rheology based on D_{Si}. A water content (C_{H2O}) exponent of only 1/3 was found for D_{Si}, which is strikingly lower than 1.2 suggested by previous deformation experiments [*Hirth and Kohlstedt*, 2003; *Karato and Jung*, 2003].

Oxygen is the second slowest diffusion species with a similar diffusion rate as silicon in most mantle minerals [*Costa and Chakraborty*, 2008; *Dobson et al.*, 2008; *Shimojuku et al.*, 2009]. It is thus expected that oxygen diffusion may also play an essential role in the creep of olivine.

Costa and Chakraborty [2008] investigated the effect of water on oxygen self-diffusion coefficients (D_O) in olivine. By comparing the results measured at 2 GPa and C_{H2O} of 30–50 weight ppm with those determined at ambient pressure under dry conditions [*Dohmen et al.*, 2002], they concluded that even ~45 weight ppm of water could enhance D_O by 1 order of magnitude. However, as pointed out by *Fei et al.* [2013], comparison of experimental results obtained at ambient pressure and at high pressures could lead to misinterpretations because different experimental setups have different error sources. In order to clarify the effects of water on D_O, experiments should be conducted with the same setup over a wide range of C_{H2O} under constant pressure and temperature conditions.

In this study, we systematically measured D_O in a forsterite single crystal at 8 GPa, 1600–1800 K, and over a wide range of C_{H2O} from <1 up to ~800 weight ppm. Our results show that water has no significant effect on D_O under upper mantle conditions.

2. Methods

The experimental approach in this study is the same as that in our previous study [*Fei et al.*, 2013]. Here we briefly describe our procedures.

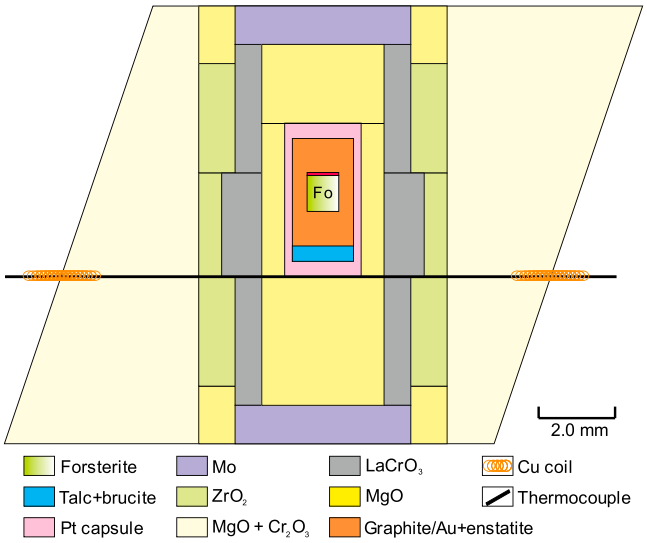

Figure 1. Cell assembly for the high-pressure experiments. Stepped $LaCrO_3$ heater was used to generate high temperature. The coated thin film for diffusion couple (red) and the thermocouple junction locate at the two $LaCrO_3$ steps to minimize the temperature measurement uncertainty. The water source located at the bottom of the Pt capsule to avoid the reaction between forsterite and talc + brucite, whereas free water released from talc + brucite could pass through the graphite powder confirmed by the homogenous C_{H2O} distributions in the crystals after annealing.

Previous oxygen self-diffusion studies show almost the same values of D_O between natural olivine [*Gérard and Jaoul*, 1989; *Ryerson et al.*, 1989] and iron-free forsterite [*Jaoul et al.*, 1980], suggesting that the effect of iron on D_O is insignificant under upper mantle conditions. Therefore, a synthetic iron-free forsterite (Mg_2SiO_4) single crystal with Fe concentration of only ~2 weight ppm was used as the starting material. The major impurity in the crystal is ~80 weight ppm of Ir determined by laser ablation inductively coupled plasma–mass spectrometry (ICP-MS) [*Fei et al.*, 2012]. Since no anisotropy of oxygen self-diffusion rate was found in forsterite or natural olivine [*Costa and Chakraborty*, 2008; *Jaoul et al.*, 1980], the D_O along *b* crystallographic direction were measured in this study.

Disks of forsterite were cored parallel to the *b* axis from a single crystal, sealed in Pt capsules with talc + brucite water source and graphite + enstatite (or enstatite + gold) buffer, and preannealed at 1600 K and 8 GPa in a multianvil apparatus at the University of Bayreuth using the cell assembly shown in Figure 1. The annealing durations were about 50–70 h which was long enough to achieve the water equilibrium in the crystal based on the hydrogen diffusion coefficient in forsterite [*Demouchy and Mackwell*, 2003]. The water in the recovered samples were measured by Fourier transform infrared (FT-IR) spectroscopy using unpolarized light along the *b* axis, and the C_{H2O} were calculated from the infrared spectra using *Bell et al.*'s [2003] calibration. Crystals with various C_{H2O} ranging from <1 up to ~800 weight ppm (Table 1) were obtained after this preannealing by controlling the ratio of water source to the graphite/gold + enstatite buffer.

The water-doped samples were mechanically polished perpendicular to the *b* axis by diamond powder (0.25 μm grain size). Because a high-defect concentration layer (~200 nm) on the surface might be formed by this mechanical polish [*Pinilla et al.*, 2012] that may affect the apparent diffusion coefficients, sample surfaces were sequentially polished in an alkaline colloidal silica solution for 3–12 h which is sufficiently long to remove the mechanically damaged layer [*Ito and Ganguly*, 2006] and were then deposited with about 500 nm thick amorphous films with a chemical composition of ^{18}O-enriched Mg_2SiO_4. The thin films have uniform thickness and $^{18}O/^{16}O$ ratio (~0.05) examined by secondary ion mass spectrometry (SIMS) profiles from two positions on one sample with thin-film deposition but without high temperature treatment.

Each thin-film deposited sample was annealed again at 8 GPa, 1600 or 1800 K for diffusion using exactly the same experimental setup, and water dopant as that used in the corresponding water-doping experiment. For the samples with C_{H2O} <1 weight ppm (below the detection limit of FT-IR), experiments were performed using the same procedures as described above but without water source. The recovered samples remain as single crystals because of the protection by graphite/gold powder at high pressure.

The samples were slightly polished by 100–200 nm in the alkaline colloidal silica solution to reduce the surface roughness after diffusion annealing [*Fei et al.*, 2012]. The water content in each sample was examined again using FT-IR, the isotopic profiles were obtained from the CAMECA IMS-6f SIMS at the Helmholtz Centre Potsdam, and the depths of SIMS craters were measured by a 3-D confocal microscope at the University of Bayreuth. Examples of the isotope profile and SIMS crater are shown in Figures 2a and 2b, respectively.

Journal of Geophysical Research: Solid Earth

10.1002/2014JB011141

Table 1. Summary of Experimental Conditions and Results of Oxygen Self-Diffusion Coefficients[a]

Run No.	T (K)	t (h)	C_{H2O}[c] (weight ppm)	C_{H2O}[d] (weight ppm)	C_{H2O}[e] (weight ppm)	$c_1 \times 10^{-2}$	$c_\infty \times 10^{-3}$	$4D_O't$ (nm^2)	δ (nm)	Rs (nm)	$L^2(Rs)$ (nm^2)	D_O (m^2/s)	Buffer
S5045-a[b]	1600	21	<1	<1	585[f]	2.5	2.7	1.8×10^5	714	48	4.9×10^3	5.9×10^{-19}	C + En[g]
S5045-b[b]	1600	21	<1	<1	328[f]	2.4	2.6	2.3×10^5	736	61	6.9×10^3	7.4×10^{-19}	C + En
V716-a	1600	52	<1	<1	29	0.9	2.0	1.0×10^6	856	162	4.0×10^4	1.3×10^{-18}	C + En
V716-b	1600	52	<1	<1	17	1.8	2.1	1.8×10^6	479	128	2.5×10^4	2.4×10^{-18}	C + En
H3390-a[b]	1600	41	242	237	476	1.5	2.3	1.0×10^6	446	45	4.5×10^3	1.7×10^{-18}	C + En
H3390-b[b]	1600	41	242	237	906	1.9	2.4	1.2×10^6	416	28	2.7×10^3	2.1×10^{-18}	C + En
H3389-a[b]	1600	9	248	230	273	1.5	2.3	2.2×10^5	587	47	4.7×10^3	1.7×10^{-18}	C + En
H3389-b[b]	1600	9	248	230	958	2.2	2.3	3.4×10^5	342	52	5.4×10^3	2.6×10^{-18}	C + En
H3389-c[b]	1600	9	248	230	254	2.1	2.5	3.4×10^5	425	28	2.7×10^3	2.6×10^{-18}	C + En
H3394-a[b]	1600	20	248	135	52	1.9	2.1	2.5×10^5	240	26	2.5×10^3	8.5×10^{-19}	C + En
H3394-b[b]	1600	20	248	135	469	3.5	2.2	1.5×10^5	98	29	2.7×10^3	5.0×10^{-19}	C + En
V724-a	1600	18	183	114	146	1.9	2.0	3.0×10^5	899	53	5.7×10^3	1.2×10^{-18}	C + En
V724-b	1600	18	183	114	154	1.4	2.2	2.2×10^5	1076	45	4.5×10^3	8.7×10^{-19}	C + En
V723	1600	23	40	47	270	0.5	2.1	4.8×10^5	55	169	4.3×10^4	1.4×10^{-18}	C + En
V720-a	1600	27	13	12	24	2.2	2.1	1.0×10^6	960	59	6.6×10^3	2.7×10^{-18}	C + En
V720-b	1600	27	13	12	18	2.0	2.0	9.5×10^5	955	33	3.2×10^3	2.4×10^{-18}	C + En
H3507-a	1600	7	805	810	3780	1.1	1.2	3.4×10^5	66	126	2.5×10^4	3.2×10^{-18}	En[h]
H3507-b	1600	7	805	810	1485	2.5	2.1	2.0×10^5	1472	164	4.0×10^4	1.6×10^{-18}	En
H3509-a[b]	1800	5	15	12	13	1.0	1.7	1.5×10^6	130	78	1.1×10^4	2.1×10^{-17}	C + En
H3509-b[b]	1800	5	15	12	17	0.5	3.0	1.4×10^6	1301	134	2.8×10^4	1.8×10^{-17}	C + En
H3509-c[b]	1800	5	15	12	140	0.9	4.1	4.7×10^6	385	165	4.1×10^4	6.5×10^{-17}	C + En

[a]The c_1, c_∞, $4D_O't$, and δ are obtained by the least square fitting in equation (1). The Rs is the standard deviation of surface height as shown in Figure 2b measured by the 3-D confocal microscope. The $L^2(Rs)$ is calculated from Rs using the relationship of $L(Rs)$ and Rs shown in Figure 3 obtained from zero-time runs. The run no. with the same starting but different endings (e.g., V720-a and V720-b) indicate different SIMS profiles measured on the same sample. The large scatterings of D_O in H3509 and H3507 are probably caused by the large fitting uncertainties of c_1 and δ in these runs.

[b]Sample coated with ~100 nm ZrO_2 films on the ^{18}O-enriched films. We performed several diffusion experiments on samples coated with an additional ZrO_2 film to protect the isotopically enriched film following the technique introduced by *Costa and Chakraborty* [2008]. The ZrO_2-coated and non-ZrO_2-coated samples show almost the same D_O. The presence of ZrO_2 thin film thus does not affect D_O in forsterite at high pressure. This is also the case for silicon diffusion confirmed in our previous studies [*Fei et al.*, 2012, 2013].

[c]Water content before diffusion annealing measured by FT-IR.

[d]Water content after diffusion annealing measured by FT-IR.

[e]Water content after diffusion annealing measured by SIMS (from the H/Si ratio without calibration) near the sample surface where the major part of oxygen diffusion profile was obtained.

[f]Anomalously high C_{H2O} by SIMS because of the low vacuum condition for this sample (~10^{-6} Pa for S5045, whereas $<5 \times 10^{-7}$ Pa for the others).

[g]Graphite + enstatite buffer.

[h]Enstatite buffer.

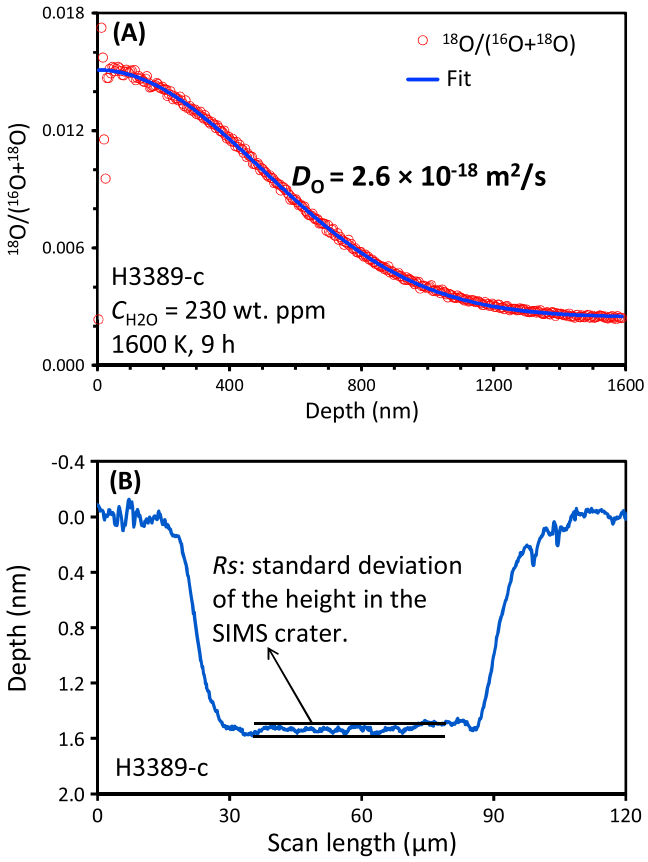

Figure 2. Examples of the apparent diffusion profile and the SIMS crater measured in the sample H3389-c annealed at 1600 K for 9 h with water content of about 230 weight ppm. (a) Diffusion profile. (b) SIMS crater. The surface data were obtained by the 3-D confocal microscope.

Since the diffusion length is comparable with the thickness of thin film in this study, the apparent diffusion coefficients were obtained by fitting the SIMS data to the finite-medium diffusion equation [*Zhang*, 2008],

$$c(x) - c_\infty = \frac{c_1 - c_\infty}{2}\left(\mathrm{erf}\frac{\delta + x}{\sqrt{4D_o' t}} + \mathrm{erf}\frac{\delta - x}{\sqrt{4D_o' t}}\right) \quad (1)$$

where $c(x)$ is the observed abundance of ^{18}O by SIMS, c_1 and c_∞ are the initial abundances of ^{18}O in the thin film and in the substrate, respectively, x is the distance from the surface, t is the annealing time, D_O' is the apparent diffusion coefficient, and δ is the extended source width [*Zhang*, 2008].

Because the coated thin film is compressed at high pressure, and the sample surface is slightly polished after diffusion by roughly 100–200 nm, it is impossible to know the exact values of δ for each sample, and therefore, the δ together with c_1, c_∞, and $4D_O't$ listed in Table 1 were obtained by the least squares fitting in equation (1). The fitting value of c_1 ranges from 0.5×10^{-2} to 3.5×10^{-2}, and δ from 55 to 1472 nm. We also tried to fix c_1 at 0.5×10^{-2} and at 3.5×10^{-2} for the fitting, or fix δ by assuming 0 or 200 nm thick layer was polished away after diffusion, and the $4D_O't$ has almost no difference (within a factor of 1.5) though the δ value varies inversely with c_1 significantly. Therefore, even though the exact values of δ and c_1 are unknown, their effects on the uncertainty of D_O are small.

Due to the slow diffusion rate of oxygen, the length of the oxygen diffusion profile is usually less than a couple of microns. The apparent diffusion profiles could thus be contributed by many factors, e.g., the surface roughness [*Fei et al.*, 2012], the SIMS convolution [*Dohmen et al.*, 2002], and so on. In order to correct these uncertainty sources, we conducted a series of zero-time diffusion experiments, in which the samples were

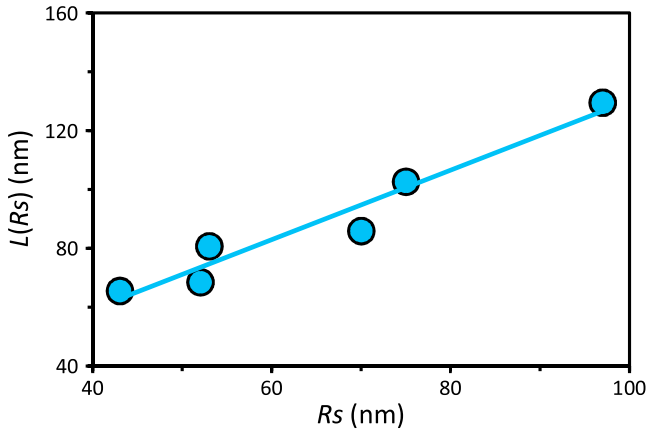

Figure 3. Relationship between nominal diffusion length and surface standard deviation as used for the error calibration. The variance of roughness was made by polishing the surfaces in the alkaline colloidal silica solution to different degrees.

compressed to 8 GPa, heated up to 1600 K, and quenched immediately. The recovered samples were polished to different degrees in surface roughness by alkaline colloidal silica solution, and the nominal diffusion profiles were measured on these samples. The nominal diffusion length (L, i.e., the nominal $(4D_O't)^{1/2}$ by fitting the profile to equation (1)) in these zero-time run samples were found to systematically increase with increasing surface roughness (Rs, here Rs is defined by the standard deviation of the surface measured in the center of SIMS crater) (Figures 2b and 3). The Rs of each real diffusion profile was measured from the SIMS crater, the $L(Rs)$ was obtained from the calibration in Figure 3, and D_O is calculated from $4D_O't$ using the calibration $4D_Ot = 4D_O't - L^2(Rs)$ [*Fei et al.*, 2012].

3. Results and Discussion

The water contents in the samples measured before and after diffusion are almost the same, suggesting a constant C_{H2O} during diffusion annealing (Table 1 and Figure 4a). Besides, in order to examine the homogeneity of C_{H2O} in the crystals, FT-IR spectra were also taken on the cross section of the sample V720, showing that the C_{H2O} has homogenous distribution in the crystals (Figure 4b) [*Fei et al.*, 2013]. In addition, the infrared spectra only give average C_{H2O} values along the thick samples, whereas the SIMS oxygen diffusion profiles were located only within several microns of the sample surfaces. Therefore, in addition to the ^{16}O and ^{18}O profiles, the ^{1}H profile was also measured concurrently by SIMS (Figure 4c), the ^{1}H concentration rapidly decreases to a constant value within a depth of ~100 nm, whereas the major part of the ^{18}O profiles for determination of D_O locates at >100 nm depth. Thus, the H concentration is not reduced or increased in the regions where the oxygen diffusion profiles were obtained. The high H concentration near the surface within 100 nm is probably because of the water absorbed during the chemical polish after diffusion [*Fei et al.*, 2012]. Furthermore, we compared the water content measured by FT-IR (C_{H2O}^{IR}) in the bulk crystals with those by SIMS (C_{H2O}^{SIMS}) near the sample surfaces where O diffusion profiles were obtained (Table 1). As shown in Figure 4d, C_{H2O}^{SIMS} is linearly proportional to C_{H2O}^{IR} when the water content is above the detection limit of SIMS. Thus, the C_{H2O} measured by FT-IR reflect the C_{H2O} values where the oxygen diffusion coefficients were measured. Although the absolute values of C_{H2O}^{SIMS} is slightly higher than C_{H2O}^{IR}, which we attribute to the lack of calibration, it does not affect the conclusion that water cannot enhance oxygen self-diffusion rate in forsterite (note that the C_{H2O} detection limit of SIMS is typically at the level of tens of weight ppm [*Rhede and Wiedenbeck*, 2006], and therefore, C_{H2O}^{SIMS} remains constant when less than tens of weight ppm in Figure 4d).

The fitted parameters of c_1, c_∞, δ, and $4D_O't$ in equation (1) are listed in Table 1, and results of D_O are plotted in Figure 5. The data points of D_O scattered by ~0.8 orders of magnitude, which is probably caused by the temperature uncertainty in the multianvil experiments (usually considered to be ±50 K, which would lead to the scattering of D_O as large as 0.7 orders of magnitude). The values of D_O at 1600 K are equivalent within experimental errors regardless of C_{H2O} in the present range. The D_O values are fitted to the Arrhenius equation,

$$D_o = A_0 C_{H_2O}^r \exp\left(-\frac{\Delta H}{RT}\right) \quad (2)$$

where A_0 is the preexponential factor, C_{H2O} is the water content in weight ppm, r is the C_{H2O} exponent, R is the ideal gas constant, T is the absolute temperature, and ΔH is the activation enthalpy. The A_0, r, and ΔH are found to be $10^{-5.9\pm1.4}$ m^2/s, 0.05 ± 0.06, and 370 ± 60 kJ/mol (the error bars are given at the 1 standard

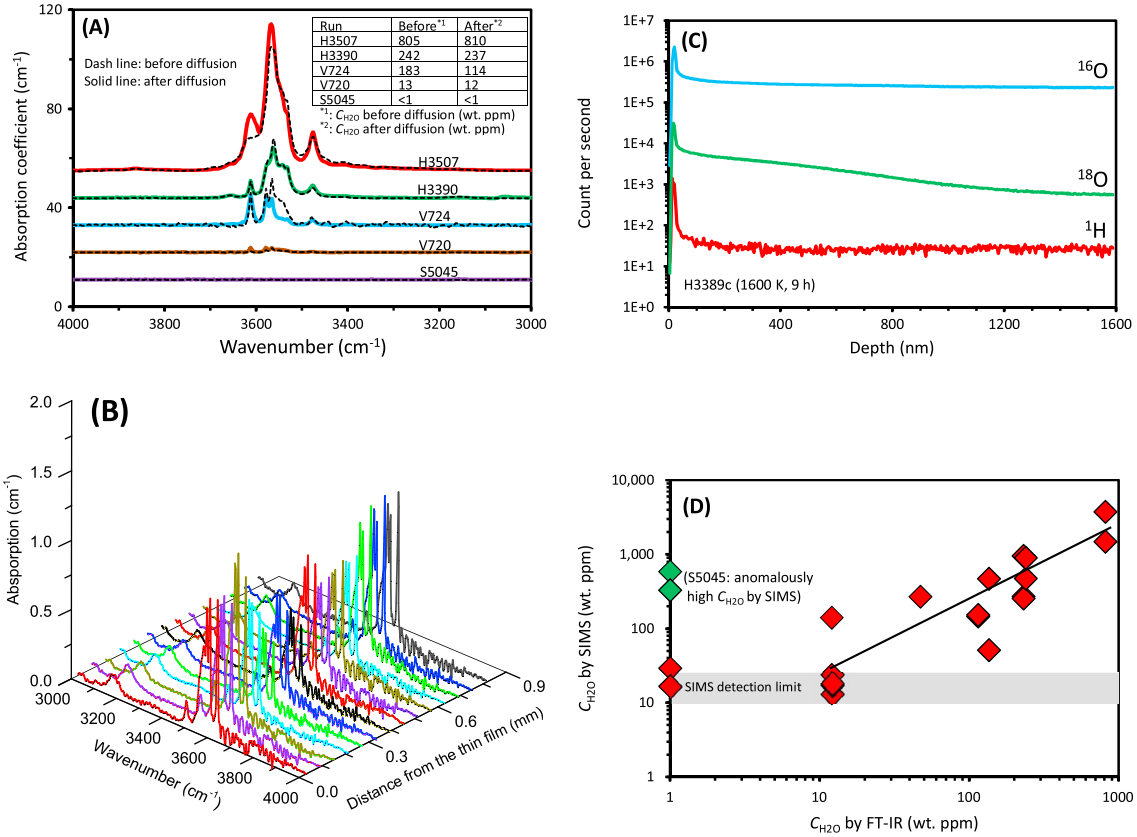

Figure 4. Water contents in the samples. (a) C_{H2O} varies from <1 up to ~800 weight ppm measured by FT-IR. The C_{H2O} before and after diffusion are essentially the same. (b) Homogenous C_{H2O} in the crystal. (c) Constant ^{1}H concentration in the location where oxygen diffusion profiles were obtained. (d) A comparison of C_{H2O} measured by FT-IR and by SIMS. The C_{H2O}^{SIMS} data are calculated from H/Si ratios (without calibration) near the regions where oxygen diffusion profiles were obtained. The detection limit of C_{H2O} by SIMS is typically at the level of tens of weight ppm [*Rhede and Wiedenbeck*, 2006], and therefore, C_{H2O}^{SIMS} remains constant when less than tens of weight ppm. The sample S5045 has worse vacuum condition (~10^{-6} Pa) than the others (<5×10^{-7} Pa), and therefore, the C_{H2O}^{SIMS} for S5045 is anomalously high. Figures 4a–4c are modified from Figure S4 in our previous study [*Fei et al.,* 2013].

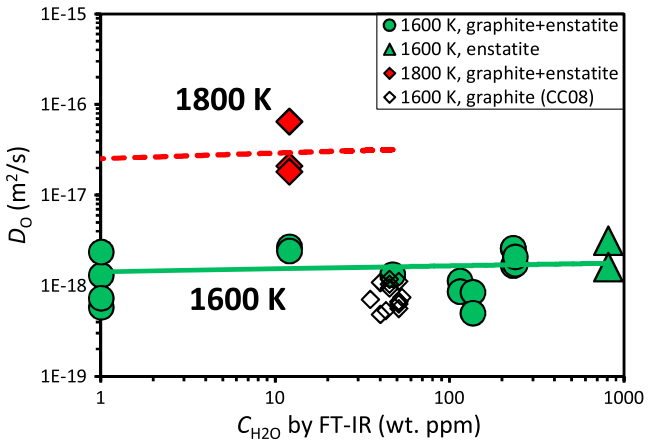

Figure 5. Plot of D_O against C_{H2O} at 8 GPa and 1600–1800 K. The C_{H2O} data under dry conditions are below the detection limit of our FT-IR equipment, which is less than 1 weight ppm. These values of D_O are plotted at C_{H2O} = 1 weight ppm. CC08: data points from *Costa and Chakraborty* [2008] corrected to 1600 K.

deviation level) by the least squares fitting, respectively. The C_{H2O} exponent for D_O is nearly zero, which means water has no significant effect on the oxygen self-diffusion rate in forsterite.

Since diffusion experiments were carried out only at two temperature conditions, the uncertainty of activation enthalpy determined in this study is thus large. By comparing the absolute values, the ΔH under wet conditions determined in this study (370 kJ/mol) is slightly higher than those under ambient pressure and dry conditions (~270–340 kJ/mol [*Andersson et al.*, 1989; *Dohmen et al.*, 2002; *Gérard and Jaoul*, 1989; *Jaoul et al.*, 1980; *Ryerson et al.*, 1989]), and

Table 2. Activation Energy for Oxygen Diffusion Determined in Forsterite and Natural Olivine (*T*: Temperature, *P*: Pressure, and ΔH: Activation Enthalpy)

Sample	C_{H2O} (weight ppm)	*T* (K)	*P* (GPa)	ΔH (kJ/mol)	Reference
Forsterite	<1–800	1600–1800	8	370 ± 60	This study
Forsterite	Dry	1423–1873	10^{-4}	320 ± 40	*Jaoul et al.* [1980]
Forsterite	Dry	1523–1793	10^{-4}	300 ± 10	*Andersson et al.* [1989]
Olivine	30–50	1473–1623	2	440 ± 20	*Costa and Chakraborty* [2008]
Olivine	Dry	1473–1673	10^{-4}	270 ± 10	*Ryerson et al.* [1989]
Olivine	Dry	1363–1773	10^{-4}	320 ± 20	*Gérard and Jaoul* [1989]
Olivine	Dry	1373–1773	10^{-4}	340 ± 10	*Dohmen et al.* [2002]
Forsterite	Computational simulation			490	*Walker et al.* [2003]

slightly lower than that determined by *Costa and Chakraborty* [2008] (~440 ± 20 kJ/mol) under wet conditions and that by *Walker et al.* [2003] (~490 kJ/mol) based on computational simulation, but still within experimental uncertainty (Table 2). On the other hand, the absolute values of D_O determined in this study at 8 GPa differ only by less than 0.4 orders of magnitude from that at 2 GPa [*Costa and Chakraborty*, 2008] (Figure 5), suggesting that the activation volume for D_O is quite small.

Natural olivine typically contains about 10% of the Fe_2SiO_4 component. The defect chemistry condition could be different if significant amount of ferric iron existed, and therefore, the water effect on D_O could be different. However, olivine crystals can accept Fe^{3+} with a very small amount as point defect ($[Fe^{3+}]/[Fe^{2+}] < 10^{-6}$ [*Karato*, 2008]). As suggested by *Kohlstedt* [2006] and *Kohlstedt et al.* [1996], the charge neutrality condition in dry iron-bearing olivine is $[Fe_{Mg}^{\bullet}] = 2[V_{Mg}'']$. With increasing C_{H2O}, it is replaced by $[(OH)_O^{\bullet}] = 2[V_{Mg}'']$ since H^+ dominates the excess positive-charged defects instead of Fe^{3+}. If C_{H2O} is high enough, the charge neutrality condition becomes $[(OH)_O^{\bullet}] = [H_{Mg}']$. Therefore, the presence of ferric iron could dominate the charge neutrality condition in olivine only under dry or relatively oxidizing conditions (i.e., $[Fe_{Mg}^{\bullet}] > [(OH)_O^{\bullet}]$) (We used the *Kröger and Vink* [1956] notation, e.g., V_{Si}'''' which indicates four effective negative charges for a vacancy in the silicon site, whereas $(OH)_O^{\bullet}$ indicates an H^+-associated O in the O site with an effective charge of +1. Square brackets [—] denote concentration of the corresponding units).

The oxygen fugacity (f_{O2}) in the enstatite-buffered samples is relatively higher in comparison to the graphite + enstatite buffered samples. However, they show almost the same value of D_O. This observation agrees with that of *Jaoul et al.* [1980], who suggested that D_O in forsterite is independent from f_{O2}. The f_{O2} dependece for D_O is found in dry iron-bearing olivine [*Gérard and Jaoul*, 1989; *Ryerson et al.*, 1989] but not in forsterite (this study and *Jaoul et al.* [1980]), which is attributed to the oxidization of Fe^{2+} to Fe^{3+}. However, the absolute values of D_O in pure forsterite (this study) are essentially the same as those in natural olivine (Fo_{92}) given by *Costa and Chakraborty* [2008] (Figure 5), both of which were obtained with C_{H2O} at the levels of tens to hundreds of weight ppm and f_{O2} using graphite buffer (correspond to the C_{H2O} and f_{O2} conditions in the upper mantle). Therefore, the difference in D_O between forsterite and natural olivine with ~10% Fe_2SiO_4 component is expected to be very small under upper mantle conditions.

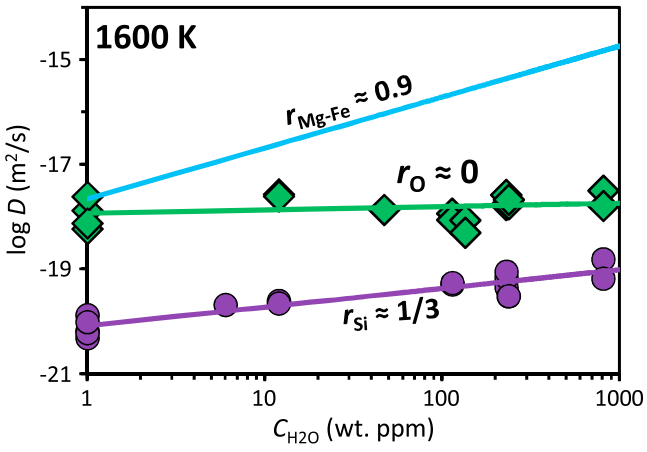

Figure 6. C_{H2O} dependences of D_O (this study), D_{Si} [*Fei et al.*, 2013], and D_{Me} [*Hier-Majumder et al.*, 2005] at 8 GPa and 1600 K. The $D_{Mg\text{-}Fe}$ data are calibrated to 8 GPa and 1600 K using an activation energy of 220 kJ/mol [*Hier-Majumder et al.*, 2005], activation volume of 7 cm^3/mol [*Holzapfel et al.*, 2007], and water fugacity converted to C_{H2O} using the calibration given by *Zhao et al.* [2004].

The water effect on D_{Si} was already found to be very small [*Fei et al.*, 2013]. In this study, we find that water has no

meaningful effect on D_O, and therefore, we have concluded that water could not significantly affect the creep rate in olivine by assuming the diffusion-controlled deformation mechanism [*Frost and Ashby*, 1982; *Weertman*, 1999] even taking into account the contribution of oxygen diffusion to creep. This is an opposite conclusion to that inferred from olivine deformation studies [*Karato et al.*, 1986; *Karato and Jung*, 2003; *Mei and Kohlstedt,* 2000a, 2000b]. As suggested in *Fei et al.* [2013], the creep rates in those deformation studies might be overestimated due to free water on grain boundaries.

We compared D_O, D_{Si}, and D_{Me} (Mg-Fe diffusion) as a function of C_{H2O} shown in Figure 6. Under dry conditions (C_{H2O} <1 weight ppm), the diffusion rates have the following relation: $D_{Mg\text{-}Fe} \approx D_O \gg D_{Si}$. Hence, the plastic deformation of olivine is controlled by Si diffusion. With C_{H2O} at the level of several hundred weight ppm, which is the case for most of the upper mantle [*Dixon et al.*, 2002; *Hirschmann*, 2006; *Workman and Hart*, 2005], $D_{Mg\text{-}Fe} \gg D_O > \approx D_{Si}$. Thus, the olivine deformation is mainly controlled by Si diffusion. On the other hand, oxygen diffusion may also play a role especially at high C_{H2O} conditions. If C_{H2O} is extremely high, which corresponds to the conditions in the mantle wedges or subducting slabs [*Iwamori and Nakakuki*, 2013; *Tonegawa et al.*, 2008], the C_{H2O} dependence of D_{Si} may become greater than an exponent of 1/3 due to the incorporation of H^+ in V_{Si}'''' [*Fei et al.*, 2013]. Though D_{Si} may rapidly increase with increasing C_{H2O}, D_O becomes comparable with or even lower than D_{Si}. In that case, the creep rate would be limited by oxygen diffusion.

In conclusion, water is not a significant factor that affects silicon and oxygen self-diffusion rates in forsterite/olivine. By assuming the diffusion-controlled deformation mechanism, the role of water in olivine creep is much smaller than previously considered.

Acknowledgments

Data supporting Figures 2–6 are available in the supporting information. We thank S. Chakraborty and R. Dohmen at Ruhr-University of Bochum for their help in sample coating and A. Yoneda at Okayama University for giving us the high-quality single crystal. We also appreciate the help of H. Keppler for FT-IR measurements, A. Audétat for ICP-MS analysis, and T. Boffa-Ballaran for single-crystal X-ray diffraction analysis. We thank all the technicians at BGI. Comments by Y. Zhang and the Associate Editor are helpful for improving the manuscript. This work is funded by the Deutche Forschungsgesellschaft (KA 3434/3-1) to T. Katsura and partly supported by the JSPS (Japan Society for the Promotion of Science) to H. Fei (P13327) and the ENB (Elite Network Bavaria) programs.

References

Andersson, K., G. Borchardt, S. Scherrer, and S. Weber (1989), Self-diffusion in Mg_2SiO_4 (forsterite) at high temperature, *Fresen. Z. Anal. Chem.*, *333*, 383–385.

Bell, D. R., G. R. Rossman, J. Maldener, D. Endisch, and F. Rauch (2003), Hydroxide in olivine: A quantitative determination of the absolute amount and calibration of the IR spectrum, *J. Geophys. Res.*, *108*(B2), 2105, doi:10.1029/2001JB000679.

Costa, F., and S. Chakraborty (2008), The effect of water on Si and O diffusion rates in olivine and implications for transport properties and processes in the upper mantle, *Phys. Earth Planet. Int.*, *166*, 11–29.

Demouchy, S., and S. Mackwell (2003), Water diffusion in synthetic iron-free forsterite, *Phys. Chem. Miner.*, *30*, 486–494.

Dixon, J. E., L. Leist, C. Langmuir, and J. Schilling (2002), Recycled dehydrated lithosphere observed in plume-influenced mid-ocean-ridge basalt, *Nature*, *420*, 385–389.

Dobson, D. P., R. Dohmen, and M. Wiedenbeck (2008), Self-diffusion of oxygen and silicon in $MgSiO_3$ perovskite, *Earth Planet. Sci. Lett.*, *270*, 125–129.

Dohmen, R., S. Chakraborty, and H. W. Becker (2002), Si and O diffusion in olivine and implications for characterizing plastic flow in the mantle, *Geophys. Res. Lett.*, *29*(21), 2030, doi:10.1029/2002GL015480.

Fei, H., C. Hegoda, D. Yamazaki, M. Wiedenbeck, H. Yurimoto, S. Shcheka, and T. Katsura (2012), High silicon self-diffusion coefficient in dry forsterite, *Earth Planet. Sci. Lett.*, *345*, 95–103.

Fei, H., M. Wiedenbeck, D. Yamazaki, and T. Katsura (2013), Small effect of water on upper mantle rheology based on Si self-diffusion coefficients, *Nature*, *498*, 213–215.

Frost, H. J., and M. F. Ashby (1982), *Deformation Mechanism Maps*, pp. 16–26, Pergamon Press, Oxford, U. K.

Gérard, O., and O. Jaoul (1989), Oxygen diffusion in San Carlos olivine, *J. Geophys. Res.*, *94*, 4119–4128, doi:10.1029/JB094iB04p04119.

Hier-Majumder, S., I. M. Anderson, and D. L. Kohlstedt (2005), Influence of protons on Fe-Mg interdiffusion in olivine, *J. Geophys. Res.*, *110*, B02202, doi:10.1029/2004JB003292.

Hirschmann, M. M. (2006), Water, melting, and the deep Earth H_2O cycle, *Annu Rev. Earth Planet. Sci.*, *34*, 629–653.

Hirth, G., and D. L. Kohlstedt (2003), Rheology of the upper mantle and the mantle wedge: A view from the experimentalists, *Geophys. Monogr.*, *138*, 83–106.

Holzapfel, C., S. Chakraborty, D. C. Rubie, and D. J. Frost (2007), Effect of pressure on Fe–Mg, Ni and Mn diffusion in $(Fe_xMg_{1-x})_2SiO_4$ olivine, *Phys. Earth Planet. Int.*, *162*, 186–198.

Houlier, B., M. Cheraghmakani, and O. Jaoul (1990), Si diffusion in San Carlos olivine, *Phys. Earth Planet. Int.*, *62*, 329–340.

Ito, M., and J. Ganguly (2006), Diffusion kinetics of Cr in olivine and ^{53}Mn–^{53}Cr thermochronology of early solar system objects, *Geochim. Cosmochim. Acta*, *70*, 799–809.

Iwamori, H., and T. Nakakuki (2013), Fluid processes in subduction zones and water transport to the deep mantle, *Phys. Chem. Deep Earth*, *373*, 372–391, doi:10.1002/9781118529492.ch13.

Jacobsen, S. D., F. Jiang, Z. Mao, T. S. Duffy, J. R. Smyth, C. M. Holl, and D. J. Frost (2008), Effect of hydration on the elastic properties of olivine, *Geophys. Res. Lett.*, *35*, L14303, doi:10.1029/2008GL034398.

Jaoul, O., C. Froidevaux, W. B. Durham, and M. Michaut (1980), Oxygen self-diffusion in forsterite: Implications for the high-temperature creep mechanism, *Earth Planet. Sci. Lett.*, *47*, 391–397.

Jung, H., and S. I. Karato (2001), Water-induced fabric transitions in olivine, *Science*, *293*, 1460–1463.

Karato, S. I. (1990), The role of hydrogen in the electrical conductivity of the upper mantle, *Nature*, *347*, 272–273.

Karato, S. I. (2008), *Deformation of Earth Materials: An Introduction to the Rheology of Solid Earth*, pp. 13–33, Cambridge Univ. Press, Cambridge, U. K.

Karato, S. I., and H. Jung (2003), Effects of pressure on high-temperature dislocation creep in olivine, *Philos. Mag.*, *83*, 401–414.

Karato, S. I., M. S. Paterson, and J. D. Fitzgerald (1986), Rheology of synthetic olivine aggregates—Influence of grain size and water, *J. Geophys. Res.*, *91*, 8151–8176, doi:10.1029/JB091iB08p08151.

Kohlstedt, D. L. (2006), The role of water in high-temperature rock deformation, *Rev. Min. Geochem.*, *62*, 377–396.

Kohlstedt, D. L., H. Keppler, and D. C. Rubie (1996), Solubility of water in the alpha, beta and gamma phases of $(Mg,Fe)_2SiO_4$, *Contrib. Min. Petrol.*, *123*, 345–357.

Kröger, F. A., and H. J. Vink (1956), Relations between the concentrations of imperfections in crystalline solids, *Solid State Phys.*, *3*, 307–435.

Mei, S., and D. L. Kohlstedt (2000a), Influence of water on plastic deformation of olivine aggregates: 1. Diffusion creep regime, *J. Geophys. Res.*, *105*, 21,457–21,469, doi:10.1029/2000JB900179.

Mei, S., and D. L. Kohlstedt (2000b), Influence of water on plastic deformation of olivine aggregates: 2. Dislocation creep regime, *J. Geophys. Res.*, *105*, 21,471–21,481, doi:10.1029/2000JB900180.

Pinilla, C., S. A. Davis, T. B. Scott, N. L. Allan, and J. D. Blundy (2012), Interfacial storage of noble gases and other trace elements in magmatic systems, *Earth Planet. Sci. Lett.*, *319*, 287–294.

Rhede, D., and M. Wiedenbeck (2006), SIMS quantification of very low hydrogen contents, *Appl. Surf. Sci.*, *252*, 7152–7154.

Ryerson, F. J., W. B. Durham, D. J. Cherniak, and W. A. Lanford (1989), Oxygen diffusion in olivine: Effect of oxygen fugacity and implications for creep, *J. Geophys. Res.*, *94*, 4105–4118, doi:10.1029/JB094iB04p04105.

Shimojuku, A., T. Kubo, E. Ohtani, T. Nakamura, R. Okazaki, R. Dohmen, and S. Chakraborty (2009), Si and O diffusion in $(Mg,Fe)_2SiO_4$ wadsleyite and ringwoodite and its implications for the rheology of the mantle transition zone, *Earth Planet. Sci. Lett.*, *284*, 103–112.

Shimojuku, A., T. Kubo, E. Ohtani, T. Nakamura, and R. Okazaki (2010), Effects of hydrogen and iron on the silicon diffusivity of wadsleyite, *Phys. Earth Planet. Int.*, *183*, 175–182.

Tonegawa, T., K. Hirahara, T. Shibutani, H. Iwamori, H. Kanamori, and K. Shiomi (2008), Water flow to the mantle transition zone inferred from a receiver function image of the Pacific slab, *Earth Planet. Sci. Lett.*, *274*, 346–354.

Walker, A. M., K. Wright, and B. Slater (2003), A computational study of oxygen diffusion in olivine, *Phys. Chem. Miner.*, *30*, 536–545.

Wang, Z., T. Hiraga, and D. L. Kohlstedt (2004), Effect of H^+ on Fe-Mg interdiffusion in olivine, $(Fe, Mg)_2SiO_4$, *Appl. Phys. Lett.*, *85*, 209–211.

Weertman, J. (1999), Microstructural mechanisms of creep, in *Mechanics and Materials: Fundamentals and Linkages*, edited by M. A. Meyers, R. W. Armstrong, and H. Kirschner, pp. 451–488, Wiley, New York.

Workman, R. K., and S. R. Hart (2005), Major and trace element composition of the depleted MORB mantle (DMM), *Earth Planet. Sci. Lett.*, *231*, 53–72.

Yoshino, T., T. Matsuzaki, A. Shatskiy, and T. Katsura (2009), The effect of water on the electrical conductivity of olivine aggregates and its implications for the electrical structure of the upper mantle, *Earth Planet. Sci. Lett.*, *288*, 291–300.

Zhang, Y. (2008), *Geochemical Kinetics*, pp. 173–324, Princeton Univ. Press, Princeton.

Zhao, Y., S. B. Ginsberg, and D. L. Kohlstedt (2004), Solubility of hydrogen in olivine: Dependence on temperature and iron content, *Contrib. Min. Petrol.*, *147*, 155–161.